

The role of interference in unraveling the ZZ -couplings of the newly discovered boson at the LHC

Mingshui Chen,¹ Tongguang Cheng,¹ James S. Gainer,^{1,*} Andrey Korytov,¹
 Konstantin T. Matchev,¹ Predrag Milenovic,¹ Guenakh Mitselmakher,¹
 Myeonghun Park,^{2,†} Aurelijus Rinkevicius,¹ and Matthew Snowball¹

¹*Physics Department, University of Florida, Gainesville, FL 32611, USA.*

²*CERN Physics Department, Theory Division, CH-1211 Geneva 23, Switzerland.*

(Dated: October 2, 2013)

Abstract

We present a general procedure for measuring the tensor structure of the coupling of the scalar Higgs-like boson recently discovered at the LHC to two Z bosons, including the effects of interference among different operators. To motivate our concern with this interference, we explore the parameter space of the couplings in the effective theory describing these interactions and illustrate the effects of interference on the differential dilepton mass distributions. Kinematic discriminants for performing coupling measurements that utilize the effects of interference are developed and described. We present projections for the sensitivity of coupling measurements that use these discriminants in future LHC operation in a variety of physics scenarios.

* Corresponding author: gainer@phys.ufl.edu

† Corresponding author: Myeonghun.Park@cern.ch

I. INTRODUCTION

As the new particle discovered by the ATLAS [2] and CMS [3] collaborations appears to be similar to the Standard Model (SM) Higgs boson [4–9], it becomes very important to measure its properties as precisely as possible in order to find or constrain physics beyond the SM. The recent ATLAS and CMS results strongly suggest that the newly discovered boson has spin zero [10–14], which we take as the starting point in the studies presented in this report. There is a large body of literature [15–53] advocating the great potential of $X \rightarrow ZZ \rightarrow 4\ell$ decays for disentangling the spin-parity properties of resonances decaying to two Z bosons and for refining the methodology for doing such measurements. In this work we explore the sensitivity of future LHC analyses to interference between various operators in this channel. We follow the framework of Ref. [49], which is briefly reviewed below.

A. Review of Framework

We consider a spin zero state X , which in general is a linear combination of a CP -even state, H , and a CP -odd state, A :

$$X \equiv H \cos \alpha + A \sin \alpha. \quad (1)$$

The couplings of the arbitrary spin zero boson, X , to two Z bosons can be described by the symmetry properties of the corresponding operators, which fall into the following three categories: (i) CP -even terms which clearly violate gauge invariance, (ii) CP -even terms which may preserve gauge invariance, (iii) CP -odd terms. For each category, the lowest dimensional operators in the effective theory, in terms of some new physics scale Λ , yield the Lagrangian

$$\mathcal{L} \supset -\left(\frac{g_1 M_Z^2}{v}\right) H Z_\mu Z^\mu - \left(\frac{g_2}{2\Lambda}\right) H F_{\mu\nu} F^{\mu\nu} - \left(\frac{g_4}{2\Lambda}\right) A F_{\mu\nu} \tilde{F}^{\mu\nu}, \quad (2)$$

where $\tilde{F}_{\mu\nu} = \frac{1}{2}\epsilon_{\mu\nu\rho\sigma} F^{\rho\sigma}$ and the g_i are dimensionless coupling constants. Re-expressing the Lagrangian terms in Eq. (2) to involve the mass eigenstate X , we obtain

$$\mathcal{L} \supset -X \left[\kappa_1 \frac{M_Z^2}{v} Z_\mu Z^\mu + \frac{\kappa_2}{2v} F_{\mu\nu} F^{\mu\nu} + \frac{\kappa_3}{2v} F_{\mu\nu} \tilde{F}^{\mu\nu} \right], \quad (3)$$

where

$$\kappa_1 = g_1 \cos \alpha, \quad \kappa_2 = g_2 \cos \alpha (v/\Lambda), \quad \kappa_3 = g_4 \sin \alpha (v/\Lambda). \quad (4)$$

TABLE I. Comparison of notations for the effective XZZ couplings.^a

Ref. [49]	κ_1	κ_2	κ_3
Refs. [27, 39]	$(i/2)g_1^{(0)}$	$-ig_2^{(0)}$	$-ig_4^{(0)}$
Ref. [44]	$(g_{1z}/2)(v/M_Z^2)$	$(g_{2z}/2)v$	$(g_{4z}/2)v$
Ref. [54]	$gv/(2M_Z)$	$g\lambda v/(2M_Z)$	$-g\lambda'v/(2M_Z)$
Ref. [55]	$-(g_{HZZ}k_{SM}v \cos \alpha)/(2M_Z^2)$	$(k_{HZZ}v \cos \alpha)/(2\Lambda)$	$(k_{AZZ}v \sin \alpha)/(2\Lambda)$

^a We note that an overall phase in the amplitude, which can be seen in this table as an overall phase in the couplings, is irrelevant except in the likely-negligible case of interference between, e.g., the $gg \rightarrow X \rightarrow ZZ^* \rightarrow 4\ell$ signal, and the loop-induced $gg \rightarrow ZZ^* \rightarrow 4\ell$ background [56–59].

Each case where exactly one of the coefficients κ_i is non-vanishing corresponds to a specific pure state: (i) $\kappa_1 \neq 0$ corresponds to a SM-like Higgs (in particular $\kappa_1 = 1$ is the tree-level SM coupling); (ii) $\kappa_2 \neq 0$ corresponds to the state which describes a SM singlet, usually denoted with 0_h^+ [39]; (iii) $\kappa_3 \neq 0$ corresponds to a pure pseudoscalar ($J^{CP} = 0^-$).

The decay amplitude that one obtains from the Lagrangian in Eq. (3) is

$$\mathcal{A}(X \rightarrow ZZ) = -\frac{2i}{v}\epsilon_1^{*\mu}\epsilon_2^{*\nu} \left((\kappa_1 M_Z^2 - \kappa_2(p_1 \cdot p_2))g_{\mu\nu} + \kappa_2 p_\mu p_\nu + \kappa_3 \epsilon_{\mu\nu\alpha\beta} p_1^\alpha p_2^\beta \right). \quad (5)$$

Here $p_{1(2)}$ is the momentum of the intermediate Z boson labelled “1” (“2”), while $p = p_1 + p_2$ is the momentum of the X boson. We note, following, e.g., Refs. [27, 28, 39] (cf. especially Eq. (11) in Ref. [39]) that the three operators in Eq. (3) generate each of the three possible Lorentz structures in the general amplitude for the decay of X to two bosons.

1. Comparison of Conventions

Various conventions have been used in writing Lagrangians and amplitudes for the study of the $X \rightarrow ZZ$ interaction. For the convenience of the reader, Table I contains a dictionary of the couplings used in Refs. [27, 39, 44, 49, 54, 55].

2. Sensitivity to Loop-Induced Couplings

The coefficients κ_i in Eq. (5) are real, since they originate from the tree-level Lagrangian in Eq. (3). By the optical theorem, the amplitude may obtain contributions from loops with

light particles (lighter than $M_X/2 \approx 63$ GeV) such that the expression for the amplitude including loop effects is analogous to that in Eq. (5), where the effective couplings κ'_i are complex:

$$\mathcal{A}(X \rightarrow ZZ) = -\frac{2i}{v} \epsilon_1^{*\mu} \epsilon_2^{*\nu} \left((\kappa'_1 M_Z^2 - \kappa'_2 (p_1 \cdot p_2)) g_{\mu\nu} + \kappa'_2 p_\mu p_\nu + \kappa'_3 \epsilon_{\mu\nu\alpha\beta} p_1^\alpha p_2^\beta \right). \quad (6)$$

However, at least one of the κ_i must not be predominantly loop-induced, or else one runs into a contradiction with the experimental constraints. For example, consider a generic loop with some invisible new particle whose coupling to the $X(Z)$ boson is $g_{X(Z)}$. Then, naively,

$$\delta\kappa'_i = \frac{g_X g_Z^2}{16\pi^2} \times \mathcal{O}(1). \quad (7)$$

In this scenario the invisible width of the X boson is

$$\Gamma_{X,\text{inv}} = \frac{g_X^2 M_X}{16\pi} \times \mathcal{O}(1), \quad (8)$$

hence taking $\Gamma_{X,\text{inv}} \lesssim \Gamma_{X,\text{total}}^{\text{exp}} \lesssim 7$ GeV [60], we obtain $g_X \lesssim 2$. Since the gauge coupling to the Z , g_Z , should be $\lesssim 1$, we get

$$\delta\kappa'_i \lesssim 1 \times 10^{-2}. \quad (9)$$

This is about two orders of magnitude smaller than the magnitude of couplings needed to give the SM rate [49]. More stringent constraints on the $\delta\kappa'_i$ (with some caveats) may be obtained from more stringent limits on the invisible width of the Higgs [13, 51, 61–64] or the invisible width of the Z [65].¹ It is therefore well-motivated to treat the relevant couplings, κ'_i , (namely, the ones which are large enough to measure at present) as predominantly real.

B. Experimental Situation

The hypothesis of the new boson being a 100% pure pseudoscalar, 0^- , has been excluded by CMS [11, 66] and ATLAS [10, 14]. The possibility of a 100% pure 0_h^+ is also disfavored at 92% C.L. [11]. Hence, in this study we assume a non-zero value of coupling, κ_1 , and address the question of the experimental sensitivity to the presence of κ_2 and κ_3 terms in the XZZ Lagrangian.

The current limit, set by CMS [11], on the presence of a pseudoscalar contribution expressed in terms of a fractional cross section is $f_{a3} = \sigma_3/(\sigma_1 + \sigma_3) < 0.58$. Here the cross

¹ We note that increasing the number of particles running in the loop alleviates the constraints on the $\delta\kappa'_i$.

sections σ_1 and σ_3 are taken for the $4e$, 4μ , and $2e2\mu$ final states together² and correspond to 100% pure 0^+ and 0^- states, respectively. This result translates into a limit on the ratio of couplings $|\kappa_3/\kappa_1| < 6.1$. The corresponding CMS analysis was set up in such a way that it was not sensitive to the interference between the κ_3 - and κ_1 -induced amplitudes.

C. Objective

In this paper, we show that by explicitly exploiting the interference between amplitudes which involve the 0^+ , 0_h^+ , and 0^- states (corresponding to the κ_1 , κ_2 , and κ_3 terms in the Lagrangian in Eq. (3), respectively) one can boost the experimental sensitivities to the presence of an 0^- (and 0_h^+) admixture. We show that the gains become particularly large at high integrated luminosities, allowing one to probe smaller values of the κ_2 and κ_3 couplings. We also address the question of establishing the presence of the interference and evaluating its sign, should decay amplitudes associated with spin zero higher dimensional operators be detected. Recently, the importance of a proper treatment of interference was discussed in the context of a somewhat different aspect of the $H \rightarrow ZZ \rightarrow 4\ell$ channel [44]; there it was the interference associated with permutations of identical leptons in the $4e$ and 4μ final states that was considered. This interference is always included in the studies presented in this report.

II. THE PHYSICAL IMPORTANCE OF INTERFERENCE

In general, interference effects can manifest themselves in two different ways: either at the level of total cross sections (reflected in the production rate, as discussed in Sec. II A below), or at the level of differential distributions (as discussed in Sec. II B below).

² For given values of couplings κ_i and κ_j , the ratios of cross sections σ_i/σ_j ($i \neq j$) for same-fermion and different-fermion final states are different. This is due to the interference effects associated with permutations of identical fermions in the final state. Hence, one should specify which final states are used in the definition of f_{a3} .

A. The impact of interference effects on the production rate

The overall rate for $X \rightarrow ZZ \rightarrow 4\ell$ events is proportional to the partial width for $X \rightarrow ZZ$ [49]

$$\Gamma(X \rightarrow ZZ) = \Gamma_{SM} \sum_{i,j} \gamma_{ij} \kappa_i \kappa_j, \quad (10)$$

where the partial $H \rightarrow ZZ$ width predicted in the SM, Γ_{SM} , is factored out in order to define constant dimensionless coefficients γ_{ij} (with $\gamma_{ij} = \gamma_{ji}$)³

$$\gamma_{11} = 1, \quad \gamma_{22} = 0.090, \quad \gamma_{33} = 0.038, \quad \gamma_{12} = -0.250, \quad \gamma_{13} = \gamma_{23} = 0. \quad (11)$$

The presence of interference is then implied by nonzero values of the “off-diagonal” coefficients γ_{ij} with $i \neq j$. Eq. (11) shows that the overall rate is affected by interference between 0^+ and 0_h^+ , which is destructive (constructive) when κ_1 and κ_2 have the same (opposite) signs. Eq. (11) also implies that at the level of total cross sections there is no interference between 0^+ and 0^- or between 0_h^+ and 0^- .

The magnitude of interference depends on the values of the couplings κ_1 and κ_2 . Obviously, for a pure 0^+ state ($\kappa_1 \neq 0, \kappa_2 = 0$) and for a pure 0_h^+ state ($\kappa_2 \neq 0, \kappa_1 = 0$) the interference is absent. Given the values in Eq. (11), one could expect the interference effect to be maximal for

$$\frac{\kappa_2}{\kappa_1} = \frac{1}{2} \tan^{-1} \left(\frac{2\gamma_{12}}{\gamma_{11} - \gamma_{22}} \right) \simeq 3.89. \quad (12)$$

In practice, the signal rate for $X \rightarrow ZZ \rightarrow 4\ell$ production is measured from data, thus imposing one constraint through Eq. (10) on the $\{\kappa_1, \kappa_2, \kappa_3\}$ parameter space [49] (provided the production rate for the X is fixed). The constraint may be solved explicitly by a suitable change of variables, reducing the relevant $\{\kappa_i\}$ parameter space to a two-dimensional surface which can be taken to be effectively the surface of a sphere [49]. For this reason, we shall not discuss the overall rate further. Instead, we will assume in our analyses that the rate measurement has already been performed and the couplings κ_i have been chosen so that they satisfy the constraint of Eq. (10).

³ The values quoted in Eq. (11) correspond to the $2e2\mu$ channel before cuts. For the $4e$ or 4μ channels (or with cuts) the numerical values are similar but not identical [49].

B. The impact of interference effects on differential distributions

Even if the overall rate is kept fixed, the interference effects are still present at the level of differential distributions (the size of this effect will be quantified in Sec. IV below). In general, the kinematics of $X \rightarrow ZZ \rightarrow 4\ell$ events is described in the X rest frame by 7 independent degrees of freedom, and interference will impact the differential distribution in this 7-dimensional signature space. For simplicity, in this subsection we will focus only on the M_{Z_1} and M_{Z_2} invariant mass distributions and use them to illustrate the effects of interference.⁴ In order to provide an intuitive understanding of some of the results to follow in Sec. IV, we shall derive analytical formulas for the M_{Z_1} and M_{Z_2} distributions, which explicitly demonstrate the interference effects.

The doubly differential decay width with respect to M_{Z_1} and M_{Z_2} can be written as

$$\frac{d^2 \Gamma}{dM_{Z_1} dM_{Z_2}} = \frac{1}{v} \sum_{i,j} \kappa_i \kappa_j F_{ij}(M_{Z_1}, M_{Z_2}; M_X), \quad (13)$$

where the dimensionless⁵ functions F_{ij} are symmetric with respect to their indices: $F_{ij} = F_{ji}$.

In the absence of any selection criteria, the functions F_{ij} are

$$F_{11}(M_{Z_1}, M_{Z_2}) = \frac{M_Z^4}{M_{Z_1}^2 M_{Z_2}^2} (x + 3) \xi(M_{Z_1}, M_{Z_2}; M_X), \quad (14)$$

$$F_{12}(M_{Z_1}, M_{Z_2}) = \frac{M_Z^2}{M_{Z_1} M_{Z_2}} 3\sqrt{x+1} \xi(M_{Z_1}, M_{Z_2}; M_X), \quad (15)$$

$$F_{22}(M_{Z_1}, M_{Z_2}) = (2x + 3) \xi(M_{Z_1}, M_{Z_2}; M_X), \quad (16)$$

$$F_{13}(M_{Z_1}, M_{Z_2}) = 0, \quad (17)$$

$$F_{23}(M_{Z_1}, M_{Z_2}) = 0, \quad (18)$$

$$F_{33}(M_{Z_1}, M_{Z_2}) = 2x \xi(M_{Z_1}, M_{Z_2}; M_X), \quad (19)$$

where the dimensionless common factor ξ is given by

$$\xi(M_{Z_1}, M_{Z_2}; M_X) \equiv \left(\frac{g_2^2(g_a^2 + g_v^2)}{2 \cos^2 \theta_W^2} \right)^2 \frac{M_{Z_1}^6 M_{Z_2}^6 \sqrt{x}}{9(2\pi)^5 v M_X^3 P_1 P_2}. \quad (20)$$

⁴ Note the webpage <http://yichen.me/project/GoldenChannel/> created by the authors of Ref. [46], may

be used to make plots of interesting differential distributions for different values of the couplings κ_i .

⁵ Since κ_i are already dimensionless, in the right-hand side of Eq. (13) we factor out $1/v$ to make F_{ij} dimensionless as well.

Here g_2 is the $SU(2)_W$ gauge coupling constant, $g_v = -\frac{1}{2} + 2 \sin \theta_W^2$, $g_a = -\frac{1}{2}$, θ_W is the Weinberg angle,

$$x \equiv \left(\frac{M_X^2 - M_{Z_1}^2 - M_{Z_2}^2}{2M_{Z_1}M_{Z_2}} \right)^2 - 1 \quad (21)$$

is a dimensionless parameter introduced in Ref. [39], and

$$P_i \equiv (M_{Z_i}^2 - M_Z^2)^2 + \Gamma_Z^2 M_Z^2 \quad (22)$$

are the Z propagator functions which depend on the mass, M_Z , and width, Γ_Z , of the Z -boson.

The doubly differential distribution in Eq. (13) is an interesting object to study experimentally and CMS and ATLAS have published plots of the Higgs candidate events in the (M_{Z_1}, M_{Z_2}) plane. Events are expected to be clustered around $M_{Z_1} = M_Z$, while the M_{Z_2} dependence is non-trivial and contains interesting information [44]. Therefore we integrate the expression in Eq. (13) over M_{Z_1} and consider instead the corresponding one dimensional distribution

$$\frac{d\Gamma}{dM_{Z_2}} \equiv \int dM_{Z_1} \left(\frac{d^2\Gamma}{dM_{Z_1}dM_{Z_2}} \right) \equiv \sum_{i,j} \kappa_i \kappa_j f_{ij}(M_{Z_2}; M_X), \quad (23)$$

with newly defined dimensionless functions

$$f_{ij}(M_{Z_2}; M_X) \equiv \frac{1}{v} \int dM_{Z_1} F_{ij}(M_{Z_1}, M_{Z_2}; M_X) \quad (24)$$

in place of Eqs. (14-19). Comparison of Eq. (10) and Eq. (13) shows that the normalization of the functions F_{ij} and f_{ij} is given by the values of the coefficients γ_{ij} in Eq. (11) [49]

$$\gamma_{ij} = \frac{1}{v \Gamma_{SM}} \int dM_{Z_1} \int dM_{Z_2} F_{ij}(M_{Z_1}, M_{Z_2}; M_X) \quad (25)$$

$$= \frac{1}{\Gamma_{SM}} \int dM_{Z_2} f_{ij}(M_{Z_2}; M_X). \quad (26)$$

Fig. 1 shows the four non-vanishing functions f_{11} (blue), f_{12} (green), f_{22} (red) and f_{33} (magenta) as a function of M_{Z_2} for the nominal value of $M_X = 125$ GeV. The two functions f_{13} and f_{23} vanish due to the CP properties of the operators considered in the Lagrangian in Eq. (3). All functions in panel (a) are normalized to unity, which makes it easier to study the differences in their shapes. In panel (b) the functions are properly normalized in accordance with Eq. (26).

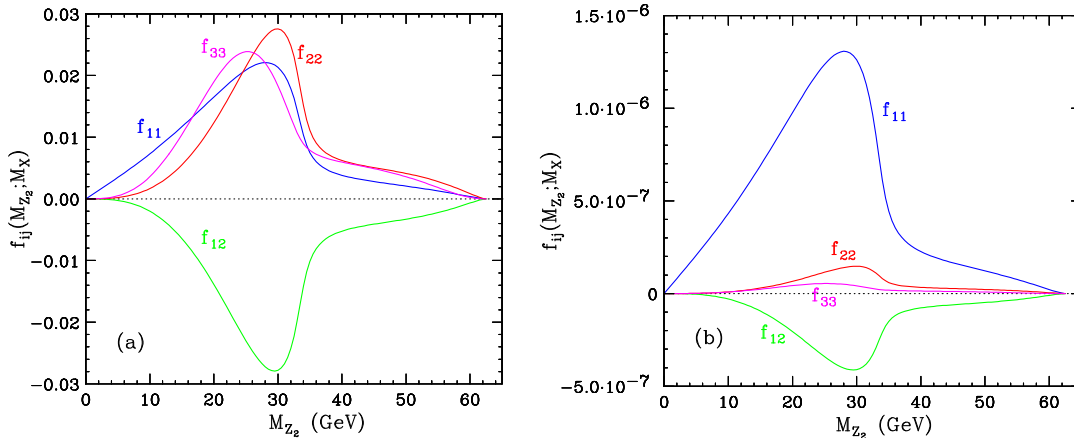


FIG. 1. The four non-vanishing functions f_{ij} defined in Eq. (24) as a function of M_{Z_2} , with $M_X = 125$ GeV and (a) unit normalization or (b) properly normalized as in Eq. (26).

Fig. 1(a) shows that all four functions exhibit similar dependence on M_{Z_2} . At first, they all monotonically increase from 0 at $M_{Z_2} = 0$, reaching a peak somewhere in the neighborhood of $M_{Z_2} \sim 25 - 30$ GeV, followed by a sudden drop at around $M_{Z_2} \sim 34$ GeV, and a long tail until $M_{Z_2} = 62.5$ GeV. This behavior can be understood purely in terms of kinematics. The majority of the events contain an on-shell Z -boson with $M_{Z_1} \approx M_Z$, which leaves only up to $M_X - M_Z \sim 34$ GeV available to M_{Z_2} , which explains the kinematic endpoint at $M_{Z_2} \sim 34$ GeV. The tail results from events where both Z -bosons are off-shell, and extends to half the X mass, $M_X/2 = 62.5$ GeV. Finally, the distributions peak relatively close to the $M_{Z_2} \sim 34$ GeV endpoint, since the propagator functions in Eq. (22) prefer M_{Z_2} to be as close as possible to the mass M_Z of the Z -boson⁶.

Fig. 1(b) compares the relative size of the different f_{ij} functions. We see that the overall magnitude is largest for f_{11} and smallest for f_{33} . Note that the interference contribution from f_{12} has the second largest magnitude and an opposite sign compared to the other three functions shown in the plot — these two facts will be important in the discussion to follow.

The observable M_{Z_2} distribution is obtained by a suitable superposition of the individual contributions seen in Fig. 1(b), properly weighted by products of κ_i couplings as specified in Eq. (23). Fig. 1 allows us to understand the resulting M_{Z_2} shapes. First, we concentrate on the location of the peak of the total M_{Z_2} distribution, which has been suggested as an

⁶ Contrast this to the case of the SM background, where there is a contribution from a virtual photon which dominates and causes the M_{Z_2} distribution to peak at much lower values [39, 44].

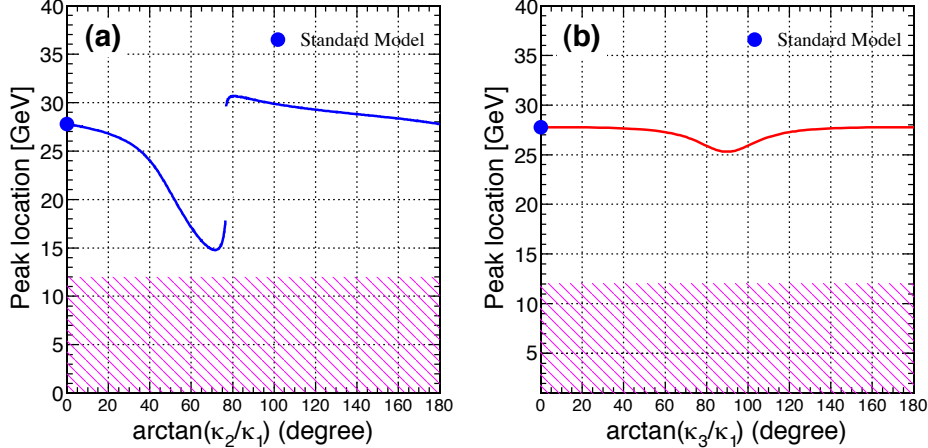


FIG. 2. The location of the peak in the M_{Z_2} distribution as a function of (a) the ratio κ_2/κ_1 , with $\kappa_3 = 0$ and (b) the ratio κ_3/κ_1 , with $\kappa_2 = 0$. The shaded region denotes the lower cut on M_{Z_2} used in our analysis. The blue circle corresponds to the case of the tree-level SM ($\kappa_1 = 1$, $\kappa_2 = 0$, $\kappa_3 = 0$).

easily measurable global observable characterizing any invariant mass distribution [67]. The peak location is plotted in Fig. 2 for two scenarios: (a) $\kappa_3 = 0$ and varying the ratio κ_2/κ_1 , keeping the total $X \rightarrow ZZ \rightarrow 4\ell$ partial width fixed to Γ_{SM} ; and (b) $\kappa_2 = 0$ and similarly varying the ratio κ_3/κ_1 .

Let us first focus on the interplay between the κ_1 and κ_3 terms in the Lagrangian (3). In this case, the behavior of the peak shown in Fig. 2(b) is relatively simple, due to the absence of an interference contribution ($f_{13} = 0$). The case of the SM (denoted by the blue circle) corresponds to $\kappa_1 = 1$ and $\kappa_3 = 0$, in which case the M_{Z_2} distribution is made up entirely of the f_{11} contribution, which peaks around 28 GeV. As the value of κ_3 is gradually increased, one introduces a larger fraction of the f_{33} component from Fig. 1, which peaks at a lower value of M_{Z_2} , around 25 GeV. As a result, the peak location in Fig. 2(b) is initially a decreasing function of the ratio κ_3/κ_1 . Eventually, we reach the case of a pure 0^- state with $\kappa_2 \neq 0$ and $\kappa_1 = 0$, when the M_{Z_2} distribution is composed entirely of the f_{33} component and the M_{Z_2} peak is located at $M_{Z_2} \sim 25$ GeV. The right half of Fig. 2(b), where the κ_1 and κ_3 couplings are taken with a relative minus sign, is a mirror image of the left and can be understood in the same way.

Notice that the f_{11} and f_{33} contributions always enter with positive weights, κ_1^2 and κ_3^2 ,

respectively. Thus the shape of the combined M_{Z_2} distribution is a weighted average between the f_{11} and f_{33} shapes seen in Fig. 1(a), which are already very similar. As a result, the peak location stays relatively constant over the whole range of the couplings ratio κ_3/κ_1 .

In contrast, when we consider the interplay between κ_1 and κ_2 , the situation changes completely, as demonstrated by Fig. 2(a). Now the M_{Z_2} distribution is built up from three components: f_{11} , which peaks near 28 GeV, f_{22} , which peaks around 30 GeV, and f_{12} , whose magnitude peaks near 29 GeV. Given that the peaks of all these three components are very close, one might expect that the peak of the total M_{Z_2} distribution would also fall in the vicinity of 28 – 30 GeV. However, Fig. 2(a) reveals that this naive expectation is false and that in the range where the couplings κ_1 and κ_2 have the same sign, the peak location can vary from as low as 15 GeV to as high as 31 GeV. The reason for this wild behavior can be traced to the fact that the interference term, f_{12} , is significant and *opposite in sign* from f_{11} and f_{22} , so that when the couplings κ_1 and κ_2 have equal signs, it destructively interferes with the sum of the f_{11} and f_{22} terms. Even more surprisingly, as the value of κ_2 is increased relative to κ_1 , at a certain point the M_{Z_2} distribution undergoes a type of “first order phase transition”, where the location of the peak “jumps” suddenly and discontinuously from around 18 GeV to near 30 GeV, signaling the presence of at least two local maxima in the M_{Z_2} distribution.

The peculiarities exhibited in Fig. 2(a) prompt further detailed investigations. In Fig. 3 we plot the M_{Z_2} distribution (shown with a red solid line) for a series of interesting ratios κ_2/κ_1 . In each frame, we also show the three individual contributions, appropriately weighted with products of κ_i factors: f_{11} (dashed blue), f_{22} (dot-dashed orange) and the interference term f_{12} (dotted green). The top left frame represents the case of the SM with $\kappa_1 = 1$ and $\kappa_2 = 0$. The M_{Z_2} distribution is comprised entirely of the f_{11} component and peaks rather sharply around 28 GeV. As we start increasing the value of κ_2 , the (negative) interference term f_{12} begins to partially offset the f_{11} piece and shifts the peak towards lower M_{Z_2} values. At the same time, the shape of the M_{Z_2} distribution becomes deformed, while the M_{Z_2} peak becomes rather broad.

A very interesting situation occurs in the κ_i parameter region illustrated by the plots in the second row of Fig. 3. Here the cancellation between the (negative) interference term f_{12} and the (positive) f_{11} and f_{22} is near maximal (see Eq. (12)). More importantly, the resulting M_{Z_2} distribution begins to develop a second local peak at high values of $M_{Z_2} \sim 30$ GeV. As

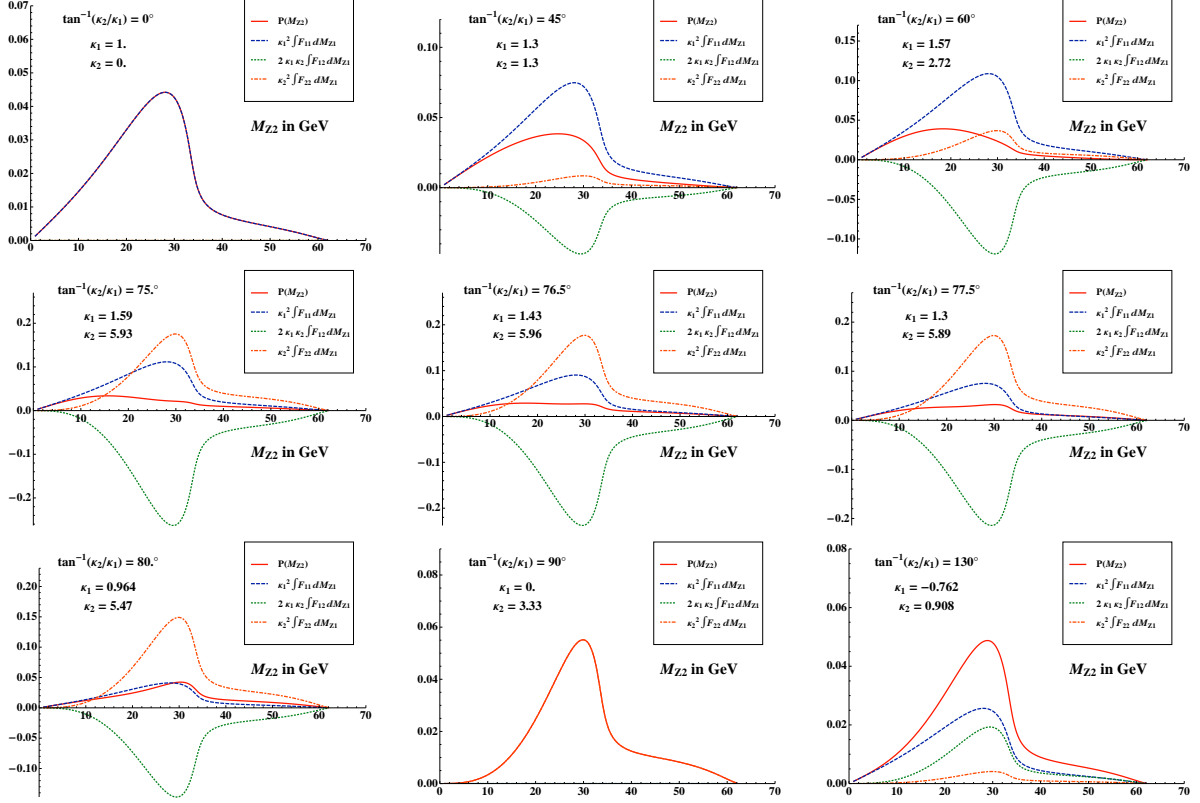


FIG. 3. M_{Z_2} distributions for $\kappa_3 = 0$ and different choices of κ_1 and κ_2 . The net total (shown in solid red) is comprised of three contributions: from f_{11} (dashed blue), from f_{22} (dot-dashed orange), and from the interference term f_{12} (dotted green). More plots like these are available in movie form at <http://www.phys.ufl.edu/~gainer/k1k2-movie.mov>.

κ_2 grows, this secondary peak becomes stronger and eventually takes over as the primary peak in the distribution, causing the sudden jump seen in Fig. 2(a). This phenomenon resembles a “first order phase transition” and can be seen more clearly in Fig. 4, where we zoom in on the actual M_{Z_2} distribution without the individual contributions. Of course, in the regime where this interesting behavior occurs, the large destructive interference also suppresses the cross section. The reader will note that the values of κ_1 and κ_2 shown in Fig. 4, which are necessary to give the correct SM partial width in Eq. (10), are relatively large as a result.

As the value of κ_2 is increased beyond the region of the “first order phase transition” shown in Fig. 4, the M_{Z_2} distribution starts to be dominated by the f_{22} contribution and eventually we get to the pure 0_h^+ state (the second to last panel in Fig. 3). The final panel

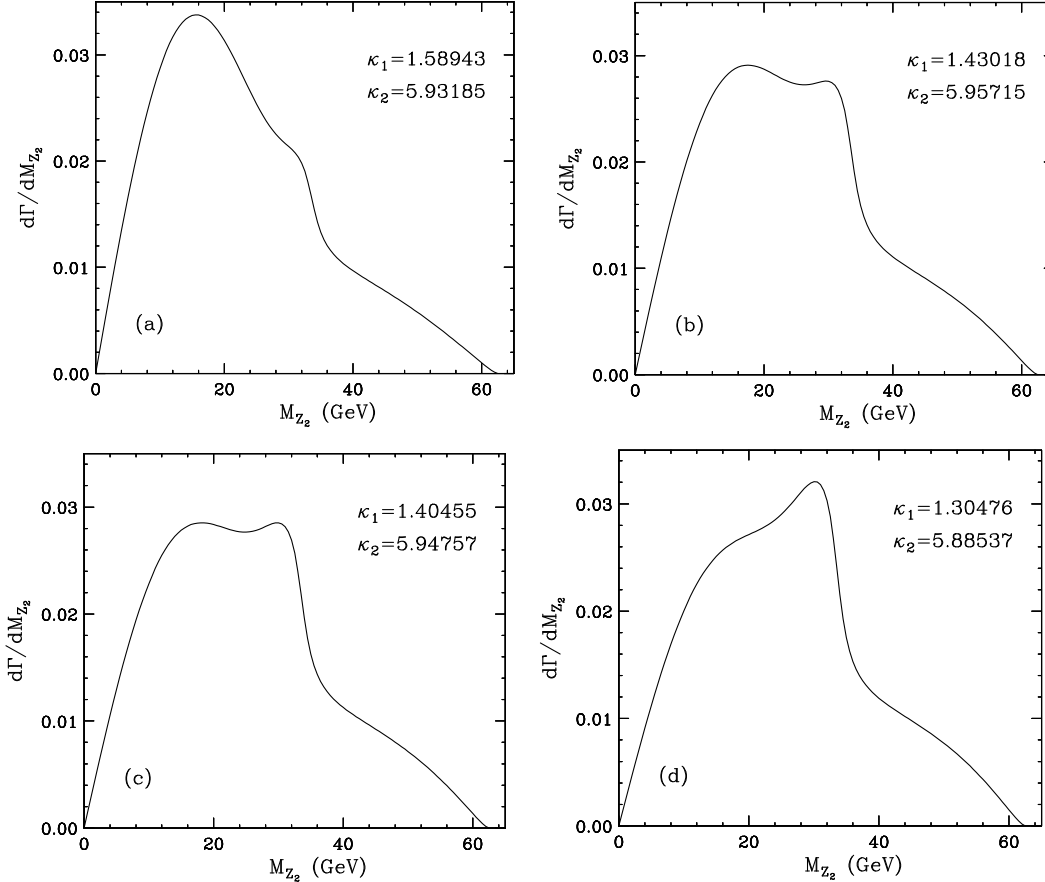


FIG. 4. Unit-normalized differential M_{Z_2} distributions for $\kappa_3 = 0$ and several choices of κ_1 and κ_2 near the point of the “first order phase transition”, where the impact of interference on the shape of the distribution is maximal (see Fig. 3).

in Fig. 3 shows a representative point with opposite signs for the couplings κ_1 and κ_2 . In that case, the sign of the interference term f_{12} is flipped and it adds constructively with f_{11} and f_{22} , causing the peak of the M_{Z_2} distribution to stay in the vicinity of 28 – 30 GeV.

III. METHODOLOGY

A. Optimized Analyses

To obtain the greatest sensitivity to a signal in a model which is characterized by a modest number of parameters, it is customary to use analyses with criteria specifically optimized for each point in the parameter space of the underlying model. This procedure

is used in all searches for Higgs bosons, whether SM or otherwise. The approach has also been advocated for SUSY searches where the signal model may have a greater number of parameters [68, 69]. In line with this idea, we introduce the kinematic discriminants that are automatically optimized for each point in the XZZ coupling parameter space.

In this report we assume that the cross section has been well-measured and that variations in the overall rate may be absorbed into the ggX couplings (provided we consider only the $pp \rightarrow X \rightarrow ZZ \rightarrow 4\ell$ channel). For this reason, the parameters we aim to measure are not the XZZ couplings, κ_i , but their ratios κ_2/κ_1 and κ_3/κ_1 . These quantities can be easily re-expressed in any desired convention, such as “geolocating” angles as in Ref. [49] or f_a -like fractions as in Ref. [11]. In this study we assume that the couplings are real numbers, as already explained in Sec. IA 2.

B. Preparation of Monte Carlo Samples

The analyses are performed using simulated $gg \rightarrow X \rightarrow ZZ \rightarrow 4\ell$ events, generated using FEYNRULES [70] and MADGRAPH [71] according to the MEKD framework [44]. This approach ensures that we include all interference effects: those arising from the presence of multiple terms in the Lagrangian as well as those associated with permutations of identical leptons in the $4e$ and 4μ final states. Following the ATLAS and CMS results [10, 11] the mass of the scalar Higgs-like boson is taken to be 125 GeV. We use MADGRAPH to simulate the $q\bar{q} \rightarrow ZZ$ backgrounds. Our simulation is performed entirely at the leading order and at the parton level. In order to compensate somewhat, we consider events with the four-lepton invariant mass in a very conservative 10 GeV mass window centered at the Higgs mass of 125 GeV (in contrast, the LHC detectors have 1 – 2% mass resolution). Consequently, the larger mass window results in the acceptance of more background events.

We use lepton kinematic selection criteria very similar to those used in the $H \rightarrow ZZ \rightarrow 4\ell$ analyses of ATLAS and CMS experiments [10, 11]. Leptons are required to have transverse momenta $p_T > 5$ GeV and pseudorapidity $|\eta| < 2.5$. At least one same-flavor opposite-sign lepton pair must have an invariant mass greater than 40 GeV, while the other lepton pair must have an invariant mass greater than 12 GeV. We use events with all three final-state combinations ($4e$, 4μ , and $2e2\mu + 2\mu2e$) in all of our analyses.

C. Projected Event Yields

In order to obtain the analysis results as a function of the integrated luminosity of the LHC runs at 14 TeV, we estimate experimental reconstruction efficiencies and contribution of the background at the 14 TeV LHC using the average of the expected signal and background event yields reported by ATLAS and CMS (Table II). The number of events expected in the 14 TeV LHC runs with $L \text{ fb}^{-1}$ of integrated luminosity, $N(L)$, is computed as:

$$N(L) = \frac{N_{\text{ATLAS}} + N_{\text{CMS}}}{2} \times \frac{\sigma(14 \text{ TeV})}{\sigma(8 \text{ TeV})} \times \frac{L}{(25 \text{ fb}^{-1})}, \quad (27)$$

The ratios of cross sections for the SM Higgs boson signal and the dominant $q\bar{q} \rightarrow ZZ$ background used in Eq. (27) are $\sigma_H(14 \text{ TeV})/\sigma_H(8 \text{ TeV}) = 2.6$ [72] and $\sigma_{ZZ}(14 \text{ TeV})/\sigma_{ZZ}(8 \text{ TeV}) = 1.9$ (computed with MCFM [73]). With these assumptions, the average expected event rates per experiment per fb^{-1} of integrated luminosity at the 14 TeV LHC are 1.9 (signal) and 0.76 (background, in the 10 GeV mass window described above).

TABLE II. The expected event yields for the SM Higgs boson signal with mass $m_H = 125 \text{ GeV}$ and background, as reported by the ATLAS and CMS collaborations for 7+8 TeV LHC Run I.

Experiment	Process	Event yield	Integrated luminosity at 7 + 8 TeV	Source
ATLAS	Signal	18.2	$4.6 + 20.7 = 25.3 \text{ fb}^{-1}$	Tab. 7 in Ref. [10]
	Bkgd	$\sim 1 \text{ event/GeV}$		Fig. 4 in Ref. [10]
CMS	Signal	19.2	$5.1 + 19.6 = 24.7 \text{ fb}^{-1}$	Tab. 2 in Ref. [11]
	Bkgd	$\sim 1 \text{ event/GeV}$		Fig. 2 in Ref. [11]

D. Kinematic Discriminants

Kinematic discriminants for separation between the two types of four-lepton processes, A and B , may be constructed by calculating the ratio of the squared matrix elements for these two hypotheses, as described in Ref. [44]. For each four-lepton event with kinematic information \mathbf{x} , one can compute:

$$D(A, B; \mathbf{x}) = \frac{|\mathcal{M}(A; \mathbf{x})|^2}{|\mathcal{M}(B; \mathbf{x})|^2}. \quad (28)$$

In our analysis, we compute the kinematic discriminants following this approach. We first consider the kinematic discriminant $D(X; 0^+)$. Here, the hypothesis “ X ” is the hypothesis that the scalar Higgs-like boson couples to Z s via both the κ_1 and κ_3 operators. We will further refer symbolically to this state as $X = \kappa_1 [0^+] + \kappa_3 [0^-]$. The hypothesis “ 0^+ ” assumes that the scalar Higgs-like boson has only the tree-level SM coupling to Z bosons. Therefore, for $D(X; 0^+)$ we obtain:

$$D(X; 0^+) = \frac{|\mathcal{M}(X)|^2}{|\mathcal{M}(0^+)|^2} = \kappa_1^2 + \kappa_3^2 \frac{|\mathcal{M}(0^-)|^2}{|\mathcal{M}(0^+)|^2} + \kappa_1 \kappa_3 \frac{(\text{interference})}{|\mathcal{M}(0^+)|^2}. \quad (29)$$

By construction, this discriminant takes into account all aspects in which kinematic distributions differ between the two hypotheses, including in particular those associated with the interference between the κ_1 and κ_3 operators in hypothesis “ X ”.

Alternatively, one can choose to use the kinematic discriminant $D(0^-; 0^+)$ [11], where the two hypotheses, “ 0^- ” and “ 0^+ ”, correspond to the cases where only the κ_3 term or only the κ_1 term are non-vanishing, respectively:

$$D(0^-; 0^+) = \frac{|\mathcal{M}(0^-)|^2}{|\mathcal{M}(0^+)|^2}. \quad (30)$$

Since the two hypotheses from which the discriminant is calculated correspond to two pure states, discriminant $D(0^-; 0^+)$ is explicitly *insensitive* to the potential effects on kinematic distributions associated with the interference (unlike discriminant $D(X; 0^+)$). The $D(0^-; 0^+)$ discriminant is optimal for comparing the two pure states or for testing for the presence of an additional pseudoscalar state nearly degenerate with the scalar Higgs-like boson (but with a sufficiently different mass that there is no significant interference in the scalar and pseudoscalar production and decays). However, as it ignores interference effects, it is not optimal for measuring the state X which couples with ZZ via both κ_1 - and κ_3 - terms. Discriminant $D(X; 0^+)$ described above is ideal for this purpose.

E. Statistical analysis

We obtain distributions for the kinematic discriminants described above using simulation. Distributions are obtained for events that correspond to the signal hypothesis “ X ”, to the signal hypothesis “ 0^+ ” (both described above) and to the background hypothesis. Examples of the distributions, $pdf(D | X + \text{bkg})$ and $pdf(D | 0^+ + \text{bkg})$ are shown in Fig. 5(a).

These kinematic discriminant distributions are then used to construct the test statistic q as follows:

$$q = -2 \ln \frac{\mathcal{L}(\text{“data”} | X + \text{bkg})}{\mathcal{L}(\text{“data”} | 0^+ + \text{bkg})} = -2 \ln \prod_i \frac{\text{pdf}(D_i | X + \text{bkg})}{\text{pdf}(D_i | 0^+ + \text{bkg})}, \quad (31)$$

where i runs over all the events in an pseudoexperiment. An example of the test statistic distributions obtained with 50000 pseudoexperiments for a particular choice of the integrated luminosity L and κ_3/κ_1 ratio is shown in Fig. 5(b).

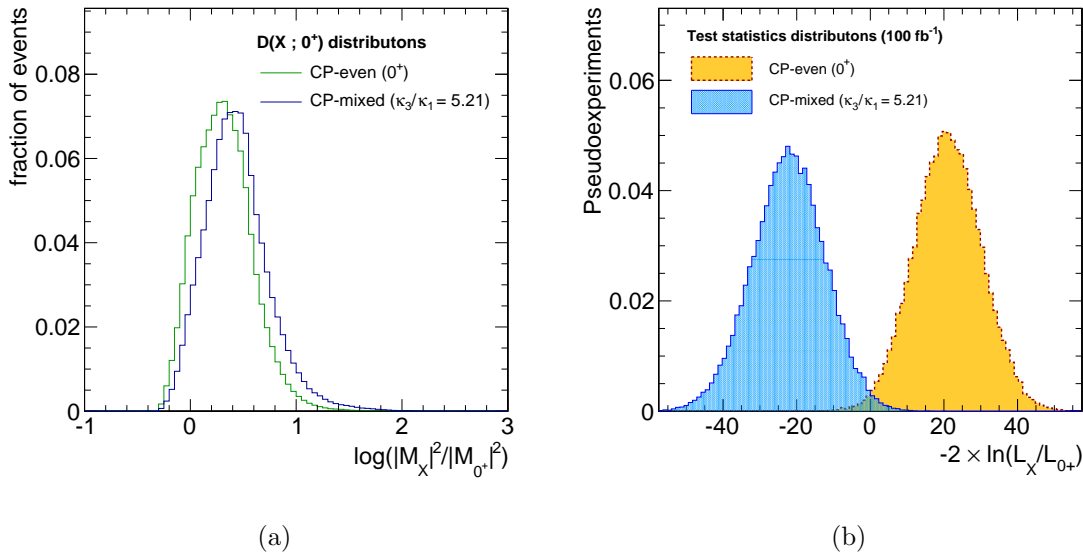


FIG. 5. (a) Distributions of $D(X; 0^+) = \frac{|\mathcal{M}(X)|^2}{|\mathcal{M}(0^+)|^2}$ for two alternative hypotheses “0⁺” and “X”, where X has $\kappa_3/\kappa_1 = 5.21$. (b) Corresponding distributions for the test statistic defined in Eq. (31) for pseudoexperiments at an integrated luminosity $L = 100 \text{ fb}^{-1}$.

To quantify the expected separation power between alternative signal hypotheses, we find a “mid-point” value, \tilde{q} , of the test statistic q between the medians of the two test statistic distributions (those generated using each signal hypothesis). We use point \tilde{q} to define two “tail probabilities”, $P(q \geq \tilde{q} | X)$ and $P(q \leq \tilde{q} | 0^+)$, in such a way that $P(q \geq \tilde{q} | X) = P(q \leq \tilde{q} | 0^+)$. This tail probability is then converted into significance \tilde{Z} (in σ) using the one-sided Gaussian tail convention:

$$P = \int_{\tilde{Z}}^{+\infty} \frac{1}{\sqrt{2\pi}} \exp(-x^2/2) dx. \quad (32)$$

Finally, for the separation power between alternative signal hypotheses we quote $Z = 2\tilde{Z}$, where the extra factor of 2 arises from the fact that the \tilde{q} point is half-way between the

medians of the two distributions. With such a definition, we treat two alternative hypotheses symmetrically and we do not need to generate billions of pseudoexperiments to assess tail probabilities corresponding to 5σ -separations.

The presence of a non-zero value of κ_3 could be established, albeit with different significances, in searches performed using either $D(X; 0^+)$ or $D(0^-; 0^+)$. The difference in the sensitivity between the two searches is manifested in case the interference between the κ_1 and κ_3 operators is present. This is not unlike the actual discovery of the Higgs boson candidate, which gave rise to the $\sim 5\sigma$ signal in the SM Higgs search [2, 3] and at the same time was also seen as $\sim 3\sigma$ excesses in the Higgs boson searches performed in the context of the fermiophobic and SM4 scenarios [74]. In case the presence of a non-zero value of κ_3 is established, the next two questions to answer are:

- whether there is one state $X = \kappa_1 [0^+] + \kappa_3 [0^-]$ with interference or there are two non-interfering states, scalar $S = \kappa_1 [0^+]$ and pseudoscalar $P = \kappa_3 [0^-]$;
- if there is interference, how well we can tell apart the relative signs of κ_3 and κ_1 couplings.

Both of these questions can be addressed by repeating the statistical analysis with properly adjusted kinematic discriminants. To demonstrate the ability of an experiment to establish the presence or absence of interference, as well as to determine the relative sign of couplings, we plot the per event log likelihood for two particular benchmark points in Figures 6 and 7. The benchmark point used for Figure 6 (Figure 7) has non-zero values for κ_1 and κ_2 (κ_1 and κ_3), while the log likelihood is evaluated for various values of the κ_2/κ_1 (κ_3/κ_1) ratio.

In the absence of interference, the likelihood functions are symmetric under $\kappa_{2,3} \rightarrow -\kappa_{2,3}$. The presence of interference breaks this symmetry and gives one sensitivity to the sign of the couplings. We note that interference between contributions to the amplitude from the κ_1 and the κ_2 terms is relatively straightforward to detect, as one would expect from the behavior of the M_{Z2} distribution discussed above. On the other side, interference involving the κ_1 and κ_3 terms will be more challenging to detect. Interestingly, it is significantly easier to determine the correct sign of κ_3 assuming interference, than it is to determine whether that interference is present.

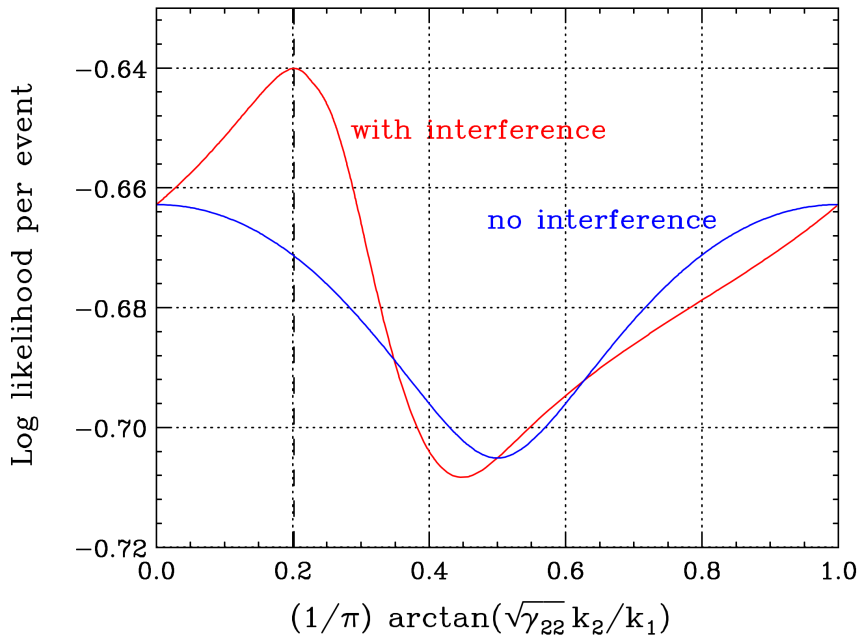


FIG. 6. The log likelihood per event for various values of κ_2/κ_1 for a particular benchmark point with $(\kappa_1, \kappa_2) \approx (1.77, 4.26)$ (vertical line), which is the point with the same cross section as SM for which $x_1 = x_2$ in the language of Ref. [49]. The quantity on the horizontal axis represents the angle along a circle of constant cross section in (κ_1, κ_2) space in the absence of interference.

IV. RESULTS

Figure 8(a) presents the expected upper limits on the ratio of couplings κ_3/κ_1 versus the integrated luminosity. Similarly, Fig. 8(b) shows a plot for the expected 5σ -observation sensitivity. Results with both the optimal $D(X; 0^+)$ and the interference-blind $D(0^-; 0^+)$ discriminants are shown. The expected exclusion and observation sensitivities are identical for positive and negative signs of the κ_3/κ_1 ratio. Of course, for a given pseudoexperiment and in the actual LHC running one sign or the other will be preferred by the data.

In Fig. 8(a) and Fig. 8(b) one can see that the sensitivities obtained with the two discriminants scale very differently with integrated luminosity L . This is because the $D(0^-; 0^+)$ discriminant does not change when one wishes to probe smaller or larger values of the κ_3/κ_1 ratio. In this case, the sensitivity to $|\kappa_3/\kappa_1|^2$ which is related to the ratio of cross sections

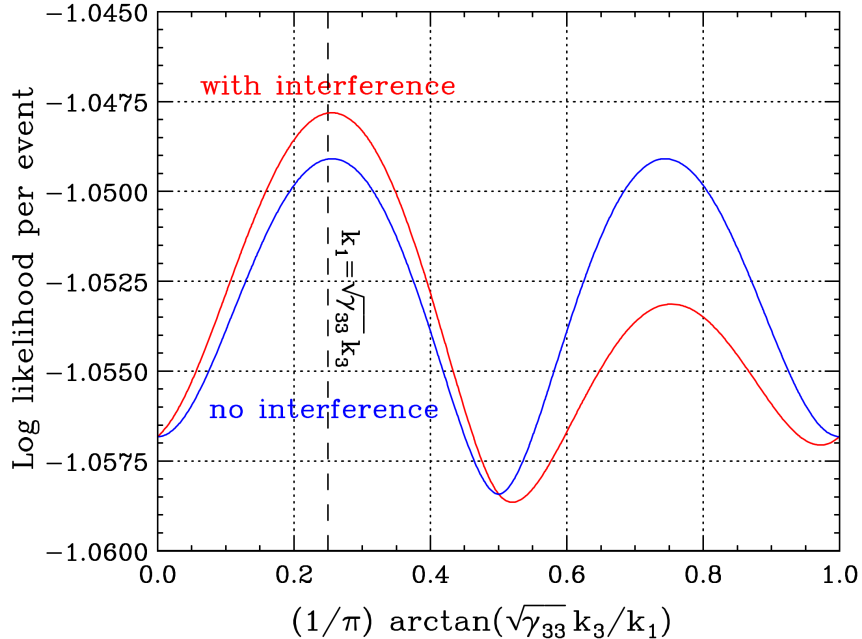


FIG. 7. The log likelihood per event for various values of κ_3/κ_1 for a particular benchmark point with $(\kappa_1, \kappa_3) = (1/\sqrt{2}, 1/\sqrt{2\gamma_{33}})$ (vertical line), which is the point with the same cross section as the standard model and an angle of $\pi/4$ with respect to the SM axis, along a circle of constant cross section in (κ_1, κ_3) space.

$\sigma_3/\sigma_1 = \gamma_{33}\kappa_3^2/\kappa_1^2$ scales approximately as $1/\sqrt{L}$. On the other hand, the $D(X;0^+)$ discriminant is automatically optimized for any given κ_3/κ_1 -value probed. For this reason analyses with $D(X;0^+)$ which probe different fractions of the 0^- state can be thought of as separate analyses, and their respective sensitivities to $|\kappa_3/\kappa_1|^2$ at different luminosities do not have to be connected via a simple $1/\sqrt{L}$ relationship.

The difference between the sensitivities obtained with the two discriminants can be quantified in terms of a ratio of integrated luminosities required to achieve the same sensitivity. Figures 8(a) and 8(b) show that this difference grows very large for smaller values of κ_3/κ_1 . For example, to probe $\kappa_3/\kappa_1 = 1$, the integrated luminosities needed for a 2σ -separation differ by a factor of 4: $\sim 700 \text{ fb}^{-1}$ with the interference-sensitive $D(X;0^+)$ discriminant versus $\sim 3000 \text{ fb}^{-1}$ with the interference-blind discriminant $D(0^-;0^+)$. With $L = 3000 \text{ fb}^{-1}$, the interference-sensitive discriminant $D(X;0^+)$ allows for reaching a 5σ -sensitivity for

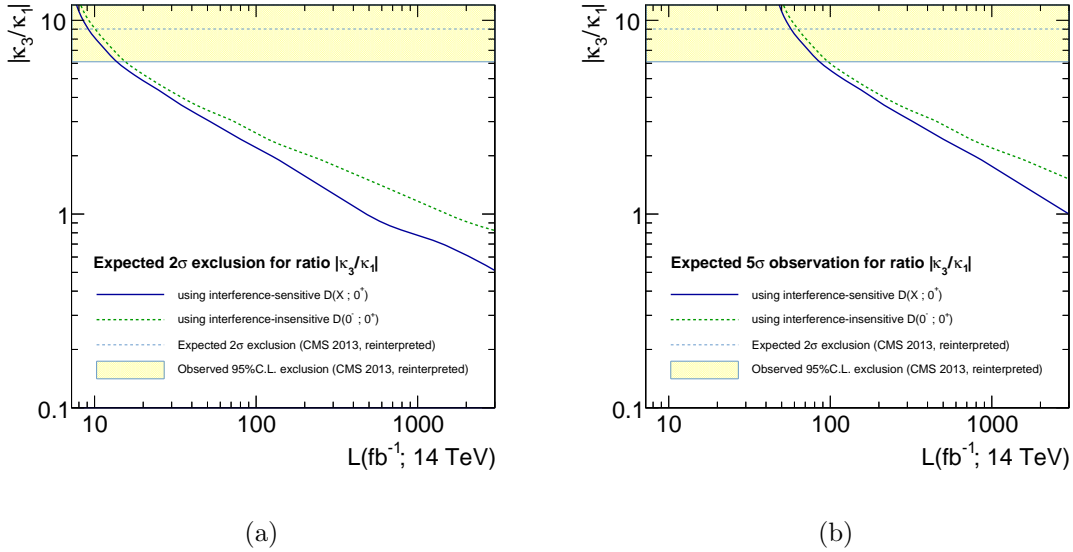


FIG. 8. (a) The integrated luminosity required for an expected 2σ -exclusion of the ratio of couplings κ_3/κ_1 , provided the data is described by the SM hypothesis. (b) The integrated luminosity required for 5σ -observation sensitivity for the ratio of couplings κ_3/κ_1 , in the presence of non-zero κ_3 . Results with interference-sensitive $D(X;0^+)$ and interference-blind $D(0^-;0^+)$ discriminants are shown with blue and green curves, respectively.

$|\kappa_3/\kappa_1| \sim 1$. However, at an integrated luminosity of 10 fb^{-1} which approximately corresponds to 25 fb^{-1} at 8 TeV, the difference in sensitivities to κ_3/κ_1 achievable with the two discriminants is rather modest, $\mathcal{O}(10\%)$.

Figure 9 shows the expected 2σ -exclusion and 5σ -observation sensitivities for the ratio of couplings κ_2/κ_1 vs. the integrated luminosity. In these figures we focus on the $\kappa_2/\kappa_1 > 0$ region for which destructive interference is present, as the prospects for early detection are more favorable with this choice of the relative sign of the two couplings. Results with both the optimal $D(X;0^+)$, where $X = \kappa_1 [0^+] + \kappa_2 [0_h^+]$, and interference-blind $D(0_h^+;0^+)$ discriminants are shown. As suggested in Eq. (12) above, there is substantial destructive interference in the range of $\kappa_2/\kappa_1 \approx 2 - 4$ that leads to dramatic changes in the M_{Z_2} invariant mass distribution shown in Fig. 3. The kinematic discriminants are automatically sensitive to such changes in the M_{Z_2} distributions, as well as to changes in other kinematic variables. As a result, it would be relatively easy to differentiate the case where κ_2/κ_1 is in this range from the pure SM Higgs-like boson. In fact, since the $\sim 25 \text{ fb}^{-1}$ of 8 TeV data already recorded on tape translates into the $\sim 10 \text{ fb}^{-1}$ of 14 TeV data, we find that the LHC

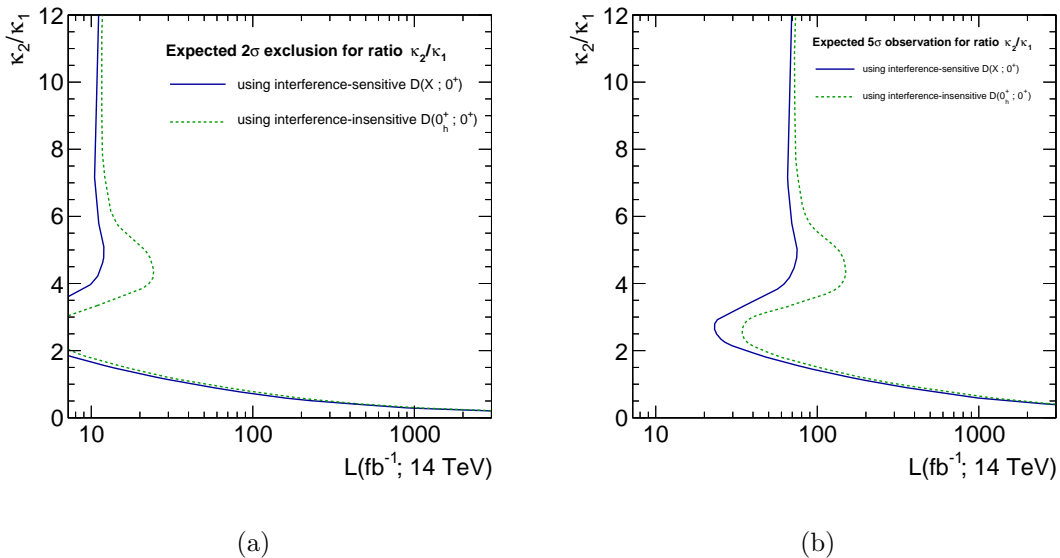


FIG. 9. (a) The integrated luminosity required for a 95% CL exclusion of the ratio of couplings κ_2/κ_1 , provided the data is described by the SM hypothesis. Results with both $D(X; 0^+)$, $X = \kappa_1 [0^+] + \kappa_2 [0_h^+]$, and interference-blind $D(0_h^+; 0^+)$ discriminants are shown. (b) Luminosity required for a 5 σ -observation of a presence of a $J^{\text{CP}} = 0_h^-$ state versus assumed ratio of couplings κ_2/κ_1 .

experiments should already be able to discover or exclude the $2 < \kappa_2/\kappa_1 < 4$ range. We note also that with existing data there should be a borderline sensitivity for exclusion of the $\kappa_2/\kappa_1 > 4$ range, which includes the case of a pure 0_h^+ state. This result is well in agreement with the expected sensitivity of 1.8 σ for a 100% pure 0_h^+ state reported by CMS [11]. The observed limit reported by CMS is 92% CL.

V. SUMMARY

We have considered the important question of how to measure the couplings of the scalar Higgs-like boson, X , to two Z bosons. In particular, we have studied the effects of the interference between various XZZ operators, presented the kinematic discriminants that take into account these interference effects, and provided projections for the coupling measurements using these discriminants at the 14 TeV LHC.

We have also compared the sensitivity of these kinematic discriminants with the kinematic discriminants that do not include interference terms and found that incorporating interference effects allows one to significantly improve the sensitivity to states where more

than one operator is present in the XZZ coupling. Depending on the value of the couplings being probed, using analyses that take interference into account may reduce the integrated luminosity required to reach a given sensitivity by as much as a factor of four, as compared with analyses that neglect this interference. Thus using analyses such as those presented may allow one to reach given sensitivity benchmarks at the LHC years earlier than otherwise.

ACKNOWLEDGEMENTS

We thank our CMS colleagues for useful discussions. M. Park is supported by the CERN-Korea fellowship through the National Research Foundation of Korea. Work supported in part by U.S. Department of Energy Grant DE-FG02-97ER41029 and NSF Grant 1007115.

-
- [1] 08, 1.
 - [2] **ATLAS** Collaboration, G. Aad *et al.*, “Observation of a new particle in the search for the Standard Model Higgs boson with the ATLAS detector at the LHC,” *Phys.Lett.* **B716** (2012) 1–29, [arXiv:1207.7214 \[hep-ex\]](#).
 - [3] **CMS** Collaboration, S. Chatrchyan *et al.*, “Observation of a new boson at a mass of 125 GeV with the CMS experiment at the LHC,” *Phys.Lett.* **B716** (2012) 30–61, [arXiv:1207.7235 \[hep-ex\]](#).
 - [4] A. Freitas and P. Schwaller, “Higgs CP Properties From Early LHC Data,” *Phys.Rev.* **D87** (2013) 055014, [arXiv:1211.1980 \[hep-ph\]](#).
 - [5] T. Corbett, O. Eboli, J. Gonzalez-Fraile, and M. Gonzalez-Garcia, “Robust Determination of the Higgs Couplings: Power to the Data,” *Phys.Rev.* **D87** (2013) 015022, [arXiv:1211.4580 \[hep-ph\]](#).
 - [6] W.-F. Chang, W.-P. Pan, and F. Xu, “An effective gauge-Higgs operators analysis of new physics associated with the Higgs,” [arXiv:1303.7035 \[hep-ph\]](#).
 - [7] B. Dumont, S. Fichet, and G. von Gersdorff, “A Bayesian view of the Higgs sector with higher dimensional operators,” [arXiv:1304.3369 \[hep-ph\]](#).
 - [8] J. Ellis and T. You, “Updated Global Analysis of Higgs Couplings,” [arXiv:1303.3879 \[hep-ph\]](#).

- [9] A. Djouadi and G. Moreau, “The couplings of the Higgs boson and its CP properties from fits of the signal strengths and their ratios at the 7+8 TeV LHC,” [arXiv:1303.6591](#) [[hep-ph](#)].
- [10] ATLAS Collaboration, “Measurements of the properties of the Higgs-like boson in the four lepton decay channel with the ATLAS detector using 25 fb⁻¹ of proton-proton collision data,” March, 2013. ATLAS-CONF-2013-013.
- [11] CMS Collaboration, “Properties of the Higgs-like boson in the decay $H \rightarrow ZZ \rightarrow 4\ell$ in pp collisions at $\sqrt{s} = 7$ and 8 TeV,” March, 2013. CMS-PAS-HIG-13-002.
- [12] ATLAS Collaboration, “Study of the spin of the new boson with up to 25 fb⁻¹ of ATLAS data,” April, 2013. ATLAS-CONF-2013-040.
- [13] CMS Collaboration, “Combination of standard model Higgs boson searches and measurements of the properties of the new boson with a mass near 125 GeV,” April, 2013. CMS-PAS-HIG-13-005.
- [14] **ATLAS Collaboration** Collaboration, G. Aad *et al.*, “Evidence for the spin-0 nature of the Higgs boson using ATLAS data,” [arXiv:1307.1432](#) [[hep-ex](#)].
- [15] C. A. Nelson, “CORRELATION BETWEEN DECAY PLANES IN HIGGS BOSON DECAYS INTO W PAIR (INTO Z PAIR),” *Phys.Rev.* **D37** (1988) 1220.
- [16] B. A. Kniehl, “THE HIGGS BOSON DECAY $H \rightarrow Z g g$,” *Phys.Lett.* **B244** (1990) 537–540.
- [17] A. Soni and R. Xu, “Probing CP violation via Higgs decays to four leptons,” *Phys.Rev.* **D48** (1993) 5259–5263, [arXiv:hep-ph/9301225](#) [[hep-ph](#)].
- [18] D. Chang, W.-Y. Keung, and I. Phillips, “CP odd correlation in the decay of neutral Higgs boson into $Z Z$, $W^+ W^-$, or $t \text{ anti-}t$,” *Phys.Rev.* **D48** (1993) 3225–3234, [arXiv:hep-ph/9303226](#) [[hep-ph](#)].
- [19] V. D. Barger, K.-m. Cheung, A. Djouadi, B. A. Kniehl, and P. Zerwas, “Higgs bosons: Intermediate mass range at $e^+ e^-$ colliders,” *Phys.Rev.* **D49** (1994) 79–90, [arXiv:hep-ph/9306270](#) [[hep-ph](#)].
- [20] T. Arens and L. Sehgal, “Energy spectra and energy correlations in the decay H to $Z Z$ to $\mu^+ \mu^- \mu^+ \mu^-$,” *Z.Phys.* **C66** (1995) 89–94, [arXiv:hep-ph/9409396](#) [[hep-ph](#)].
- [21] S. Choi, D. Miller, M. Muhlleitner, and P. Zerwas, “Identifying the Higgs spin and parity in decays to Z pairs,” *Phys.Lett.* **B553** (2003) 61–71, [arXiv:hep-ph/0210077](#) [[hep-ph](#)].

- [22] C. Buszello, I. Fleck, P. Marquard, and J. van der Bij, “Prospective analysis of spin- and CP-sensitive variables in H to $Z Z$ to $l(1)+l(1)-l(2)+l(2)-$ at the LHC,” *Eur.Phys.J.* **C32** (2004) 209–219, [arXiv:hep-ph/0212396](#) [hep-ph].
- [23] S. Schalla, “Study on the Measurement of the CP-Eigenstate of Higgs Bosons with the CMS experiment at the LHC.”.
- [24] R. M. Godbole, . Miller, D.J., and M. M. Muhlleitner, “Aspects of CP violation in the $H ZZ$ coupling at the LHC,” *JHEP* **0712** (2007) 031, [arXiv:0708.0458](#) [hep-ph].
- [25] V. Kovalchuk, “Model-independent analysis of CP violation effects in decays of the Higgs boson into a pair of the W and Z bosons,” *J.Exp.Theor.Phys.* **107** (2008) 774–786.
- [26] Q.-H. Cao, C. Jackson, W.-Y. Keung, I. Low, and J. Shu, “The Higgs Mechanism and Loop-induced Decays of a Scalar into Two Z Bosons,” *Phys.Rev.* **D81** (2010) 015010, [arXiv:0911.3398](#) [hep-ph].
- [27] Y. Gao, A. V. Gritsan, Z. Guo, K. Melnikov, M. Schulze, *et al.*, “Spin determination of single-produced resonances at hadron colliders,” *Phys.Rev.* **D81** (2010) 075022, [arXiv:1001.3396](#) [hep-ph].
- [28] A. De Rujula, J. Lykken, M. Pierini, C. Rogan, and M. Spiropulu, “Higgs look-alikes at the LHC,” *Phys.Rev.* **D82** (2010) 013003, [arXiv:1001.5300](#) [hep-ph].
- [29] C. Englert, C. Hackstein, and M. Spannowsky, “Measuring spin and CP from semi-hadronic ZZ decays using jet substructure,” *Phys.Rev.* **D82** (2010) 114024, [arXiv:1010.0676](#) [hep-ph].
- [30] A. Matsuzaki and H. Tanaka, “Determination of the Higgs CP property in Hadron Colliders,” [arXiv:1101.2104](#) [hep-ph].
- [31] U. De Sanctis, M. Fabbrichesi, and A. Tonerio, “Telling the spin of the ‘Higgs boson’ at the LHC,” *Phys.Rev.* **D84** (2011) 015013, [arXiv:1103.1973](#) [hep-ph].
- [32] J. S. Gainer, K. Kumar, I. Low, and R. Vega-Morales, “Improving the sensitivity of Higgs boson searches in the golden channel,” *JHEP* **1111** (2011) 027, [arXiv:1108.2274](#) [hep-ph].
- [33] C. Englert, M. Spannowsky, and M. Takeuchi, “Measuring Higgs CP and couplings with hadronic event shapes,” *JHEP* **1206** (2012) 108, [arXiv:1203.5788](#) [hep-ph].
- [34] J. M. Campbell, W. T. Giele, and C. Williams, “The Matrix Element Method at Next-to-Leading Order,” *JHEP* **1211** (2012) 043, [arXiv:1204.4424](#) [hep-ph].

- [35] J. M. Campbell, W. T. Giele, and C. Williams, “Extending the Matrix Element Method to Next-to-Leading Order,” [arXiv:1205.3434](#) [[hep-ph](#)].
- [36] B. A. Kniehl and O. L. Veretin, “Low-mass Higgs decays to four leptons at one loop and beyond,” *Phys.Rev.* **D86** (2012) 053007, [arXiv:1206.7110](#) [[hep-ph](#)].
- [37] J. W. Moffat, “Identification of the 125 GeV Resonance as a Pseudoscalar Quarkonium Meson,” [arXiv:1207.6015](#) [[hep-ph](#)].
- [38] B. Coleppa, K. Kumar, and H. E. Logan, “Can the 126 GeV boson be a pseudoscalar?,” *Phys.Rev.* **D86** (2012) 075022, [arXiv:1208.2692](#) [[hep-ph](#)].
- [39] S. Bolognesi, Y. Gao, A. V. Gritsan, K. Melnikov, M. Schulze, *et al.*, “On the spin and parity of a single-produced resonance at the LHC,” *Phys.Rev.* **D86** (2012) 095031, [arXiv:1208.4018](#) [[hep-ph](#)].
- [40] R. Boughezal, T. J. LeCompte, and F. Petriello, “Single-variable asymmetries for measuring the ‘Higgs’ boson spin and CP properties,” [arXiv:1208.4311](#) [[hep-ph](#)].
- [41] D. Stolarski and R. Vega-Morales, “Directly Measuring the Tensor Structure of the Scalar Coupling to Gauge Bosons,” *Phys.Rev.* **D86** (2012) 117504, [arXiv:1208.4840](#) [[hep-ph](#)].
- [42] P. Cea, “Comment on the evidence of the Higgs boson at LHC,” [arXiv:1209.3106](#) [[hep-ph](#)].
- [43] J. Kumar, A. Rajaraman, and D. Yaylali, “Spin Determination for Fermiophobic Bosons,” *Phys.Rev.* **D86** (2012) 115019, [arXiv:1209.5432](#) [[hep-ph](#)].
- [44] P. Avery, D. Bourilkov, M. Chen, T. Cheng, A. Drozdetskiy, *et al.*, “Precision studies of the Higgs boson decay channel $H \rightarrow ZZ \rightarrow 4l$ with MEKD,” *Phys.Rev. D* **87** (2013) 055006, [arXiv:1210.0896](#) [[hep-ph](#)].
- [45] E. Masso and V. Sanz, “Limits on Anomalous Couplings of the Higgs to Electroweak Gauge Bosons from LEP and LHC,” *Phys.Rev.* **D87** (2013) 033001, [arXiv:1211.1320](#) [[hep-ph](#)].
- [46] Y. Chen, N. Tran, and R. Vega-Morales, “Scrutinizing the Higgs Signal and Background in the $2e2\mu$ Golden Channel,” *JHEP* **1301** (2013) 182, [arXiv:1211.1959](#) [[hep-ph](#)].
- [47] T. Modak, D. Sahoo, R. Sinha, and H.-Y. Cheng, “Inferring the nature of the boson at 125-126 GeV,” [arXiv:1301.5404](#) [[hep-ph](#)].
- [48] S. Kanemura, M. Kikuchi, and K. Yagyu, “Probing exotic Higgs sectors from the precise measurement of Higgs boson couplings,” [arXiv:1301.7303](#) [[hep-ph](#)].

- [49] J. S. Gainer, J. Lykken, K. T. Matchev, S. Mrenna, and M. Park, “Spherical Parametrization of the Higgs Boson Candidate,” *Phys.Rev.Lett.* **111** (2013) 041801, [arXiv:1304.4936 \[hep-ph\]](#).
- [50] **The LHC Higgs Cross Section Working Group** Collaboration, S. Heinemeyer *et al.*, “Handbook of LHC Higgs Cross Sections: 3. Higgs Properties,” [arXiv:1307.1347 \[hep-ph\]](#).
- [51] F. Caola and K. Melnikov, “Constraining the Higgs boson width with ZZ production at the LHC,” [arXiv:1307.4935 \[hep-ph\]](#).
- [52] Y. Sun, X.-F. Wang, and D.-N. Gao, “CP mixed property of the Higgs-like particle in the decay channel $h \rightarrow ZZ^* \rightarrow 4l$,” [arXiv:1309.4171 \[hep-ph\]](#).
- [53] I. Anderson, S. Bolognesi, F. Caola, Y. Gao, A. V. Gritsan, *et al.*, “Constraining anomalous HVV interactions at proton and lepton colliders,” [arXiv:1309.4819 \[hep-ph\]](#).
- [54] A. Djouadi, R. Godbole, B. Mellado, and K. Mohan, “Probing the spin-parity of the Higgs boson via jet kinematics in vector boson fusion,” *Phys.Lett.* **B723** (2013) 307–313, [arXiv:1301.4965 \[hep-ph\]](#).
- [55] P. Artoisenet, P. de Aquino, F. Demartin, R. Frederix, S. Frixione, *et al.*, “A framework for Higgs characterisation,” [arXiv:1306.6464 \[hep-ph\]](#).
- [56] T. Binoth, N. Kauer, and P. Mertsch, “Gluon-induced QCD corrections to pp to ZZ to l anti-l l-prime anti-l-prime,” [arXiv:0807.0024 \[hep-ph\]](#).
- [57] S. P. Martin, “Shift in the LHC Higgs diphoton mass peak from interference with background,” *Phys.Rev.* **D86** (2012) 073016, [arXiv:1208.1533 \[hep-ph\]](#).
- [58] N. Kauer, “Inadequacy of zero-width approximation for a light Higgs boson signal,” *Mod. Phys. Lett. A, Vol. 28, No. 20* (2013) 1330015, [arXiv:1305.2092 \[hep-ph\]](#).
- [59] L. J. Dixon and Y. Li, “Bounding the Higgs Boson Width Through Interferometry,” [arXiv:1305.3854 \[hep-ph\]](#).
- [60] CMS Collaboration, “Properties of the observed Higgs-like resonance decaying into two photons,” July, 2013. CMS-PAS-HIG-13-016.
- [61] **ATLAS** Collaboration, ATLAS Collaboration, “Search for invisible decays of a Higgs boson produced in association with a Z boson in ATLAS,” 2013.
- [62] ATLAS Collaboration, “Combined coupling measurements of the Higgs-like boson with the ATLAS detector using up to 25 fb^{-1} of proton-proton collision data,” 2013.

- [63] ATLAS Collaboration, “Search for invisible decays of a Higgs boson produced in association with a Z boson in ATLAS,” 2013.
- [64] G. Belanger, B. Dumont, U. Ellwanger, J. Gunion, and S. Kraml, “Status of invisible Higgs decays,” *Phys.Lett.* **B723** (2013) 340–347, [arXiv:1302.5694 \[hep-ph\]](#).
- [65] **ALEPH Collaboration, DELPHI Collaboration, L3 Collaboration, OPAL Collaboration, SLD Collaboration, LEP Electroweak Working Group, SLD Electroweak Group, SLD Heavy Flavour Group** Collaboration, S. Schael *et al.*, “Precision electroweak measurements on the Z resonance,” *Phys.Rept.* **427** (2006) 257–454, [arXiv:hep-ex/0509008 \[hep-ex\]](#).
- [66] **CMS Collaboration**, S. Chatrchyan *et al.*, “On the mass and spin-parity of the Higgs boson candidate via its decays to Z boson pairs,” *Phys.Rev.Lett.* **110** (2013) 081803, [arXiv:1212.6639 \[hep-ex\]](#).
- [67] W. S. Cho, D. Kim, K. T. Matchev, and M. Park, “Cracking the dark matter code at the LHC,” [arXiv:1206.1546 \[hep-ph\]](#).
- [68] K. T. Matchev and D. M. Pierce, “Supersymmetry reach of the Tevatron via trilepton, like sign dilepton and dilepton plus τ jet signatures,” *Phys.Rev.* **D60** (1999) 075004, [arXiv:hep-ph/9904282 \[hep-ph\]](#).
- [69] K. T. Matchev and D. M. Pierce, “New backgrounds in trilepton, dilepton and dilepton plus τ jet SUSY signals at the Tevatron,” *Phys.Lett.* **B467** (1999) 225–231, [arXiv:hep-ph/9907505 \[hep-ph\]](#).
- [70] N. D. Christensen and C. Duhr, “FeynRules - Feynman rules made easy,” *Comput.Phys.Commun.* **180** (2009) 1614–1641, [arXiv:0806.4194 \[hep-ph\]](#).
- [71] J. Alwall, M. Herquet, F. Maltoni, O. Mattelaer, and T. Stelzer, “MadGraph 5 : Going Beyond,” *JHEP* **1106** (2011) 128, [arXiv:1106.0522 \[hep-ph\]](#).
- [72] **LHC Higgs Cross Section Working Group** Collaboration, S. Dittmaier *et al.*, “Handbook of LHC Higgs Cross Sections: 1. Inclusive Observables,” [arXiv:1101.0593 \[hep-ph\]](#).
- [73] J. M. Campbell and R. Ellis, “MCFM for the Tevatron and the LHC,” *Nucl.Phys.Proc.Suppl.* **205-206** (2010) 10–15, [arXiv:1007.3492 \[hep-ph\]](#).
- [74] **CMS Collaboration** Collaboration, S. Chatrchyan *et al.*, “Searches for Higgs bosons in pp collisions at $\sqrt{s} = 7$ and 8 TeV in the context of four-generation and fermiophobic models,”

Phys.Lett. **B725** (2013) 36–59, arXiv:1302.1764 [hep-ex].